Sputtering Deposition of P-Type SnO Films with SnO_2 Target in Hydrogen-Containing Atmosphere

Po-Ching Hsu,[†] Chao-Jui Hsu,[†] Ching-Hsiang Chang,[†] Shiao-Po Tsai,[†] Wei-Chung Chen,[†] Hsing-Hung Hsieh,[‡,§] and Chung-Chih Wu*,[†]

[†]Graduate Institute of Electronics Engineering, Graduate Institute of Photonics and Optoelectronics, Department of Electrical Engineering, and Innovative Photonics Advanced Research Center (i-PARC), National Taiwan University, Taipei, 10617, Taiwan

[‡]AU Optronics Corporation, Hsinchu Science Park, Hsinchu 300, Taiwan

ABSTRACT: In this work, we had investigated sputtering deposition of p-type SnO using the widely used and robust SnO_2 target in a hydrogen-containing reducing atmosphere. The effects of the hydrogen-containing sputtering gas on structures, compositions, optical, and electrical properties of deposited SnOx films were studied. Results show that polycrystalline and SnO-dominant films could be readily obtained by carefully controlling the hydrogen gas ratio in the sputtering gas and the extent of reduction reaction. P-type conductivity was unambiguously observed for SnO-dominant films with traceable Sn components, exhibiting a p-type Hall mobility of up to ~3 $cm^2\ V^{-1}\ s^{-1}$. P-type SnO thin-film transistors using such SnO-dominant films were also demonstrated.

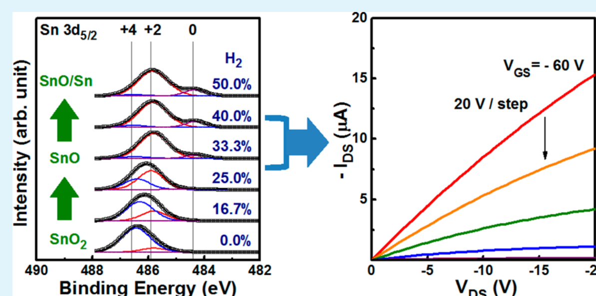

KEYWORDS: *p-type, oxide semiconductor, thin film transistor, tin monoxide, tin oxide, reactive sputtering*

1. INTRODUCTION

Thin-film transistors (TFTs) based on oxide semiconductors, because of their performance and manufacturing advantages, have been regarded as a promising next-generation TFT technology for displays and flexible electronics.[1−3] Despite the rapid development of n-type oxide TFTs in recent years, only few p-type oxide semiconductors were reported for TFTs and their properties and fabrication techniques are still far from practical applications.[4−12] P-type oxide TFTs, however, are highly desired in general so that low-power and high-performance complementary circuits can be realized by oxide TFTs and better compatibility with circuits of active-matrix organic light-emitting diode displays may be achieved.[12]

Hole conduction is generally more difficult in oxide semiconductors mainly because hole transporting paths and the valence band maxima (VBM) of oxide semiconductors are usually composed of anisotropic and strongly localized 2p orbitals of oxygen ions, often leading to limited hole mobility.[13] As such, few studies of tin monoxide (SnO) in recent years suggested it be a promising p-type oxide semiconductor.[3] Pseudoclosed 5s orbitals of Sn and 2p orbitals of O have close energy levels for effective interaction. Thus, they could form more isotropic and delocalized hybridized orbitals to compose a VBM potentially having more effective hole transport.[12,14] The first p-type SnO TFT was demonstrated using SnO epitaxially grown by pulsed laser deposition (PLD) at high temperatures. It exhibited a field-effect mobility of ~1.3 $cm^2\ V^{-1}\ s^{-1}$ and an on/off ratio of ~1×10^2.[12] P-type SnO films and TFTs had also been fabricated by more TFT-industry-compatible sputtering from the SnO target or reactive sputtering from the Sn target.[14−16] Yet both SnO and Sn targets used for sputtering deposition of p-type SnO films suffer some issues for practical applications. The SnO material (phase) itself is not thermodynamically stable at temperatures higher than 270 °C because a strong disproportionation reaction ($4SnO \rightarrow Sn_3O_4 + Sn \rightarrow 2SnO_2 + 2Sn$) would occur at such higher temperatures.[17] As such, the widely used high-temperature sintering cannot be used to fabricate pure SnO targets and one is forced to use lower-temperature pressing, which however fails to give high-density and robust SnO targets required for real uses.[15,16] On the other hand, SnO-dominant films can also be obtained by reactive sputtering with the Sn target in an oxidizing atmosphere (e.g., Ar mixed with an appropriate amount of O_2).[14] Yet Sn suffers from its low melting point, which would limit the sputtering conditions and/or the use of Sn targets in continuous/repeated sputtering, making it also not so practical. In view of these, it will be of interest to explore other alternative and more practical sputtering targets/processes for preparation of p-type SnO films.

In contrast to obtaining p-type SnO films by oxidizing Sn (as in reactive sputtering with the Sn target in the Ar/O_2 mixed atmosphere),[14] it is natural to speculate whether p-type SnO can also be prepared by a reverse process, i.e., by reducing reaction from SnO_2. For instance, it may be worthy of exploring whether p-type SnO can be obtained by sputtering with a pure SnO_2 target in a reducing atmosphere (e.g., in a hydrogen-

Received: May 22, 2014
Accepted: July 13, 2014
Published: July 18, 2014

© 2014 American Chemical Society

dx.doi.org/10.1021/am5031787 | *ACS Appl. Mater. Interfaces* 2014, 6, 13724−13729

containing atmosphere). If this is true, it will be of particular interest because SnO_2 is a widely used/available, robust/homogeneous/high-quality, and cost-effective target material. In this work, we investigate sputtering deposition of p-type SnO films with the SnO_2 target in the hydrogen-containing atmosphere. The effects of the hydrogen-containing sputtering gas on structures, compositions, optical and electrical properties of deposited SnOx films are studied. Results show that p-type SnO films exhibiting decent performance (e.g., hole mobility up to 3 $cm^2 V^{-1} s^{-1}$) indeed can be successfully achieved with such a target and sputtering technique. P-type SnO TFTs using such p-type SnO films are also demonstrated.

2. EXPERIMENTS

Using the ceramic SnO_2 target purchased (Well Being Co., Ltd., 99.99% purity), SnOx films were deposited by RF magnetron sputtering in an Ar/H_2 mixed atmosphere, with a RF power of 200 W, a working pressure of 5 mTorr typical for sputtering, and no intentional substrate heating. The flow-rate ratio of H_2 relative to Ar was adjusted to study effects of the H_2 gas ratio on characteristics of deposited SnOx films. Samples for thin-film characterization were deposited on Corning E2K glass substrates. Deposited films were subjected to postannealing at 300 °C in vacuum in a rapid thermal annealing (RTA) system for 1 h.

X-ray diffraction (XRD) analyses were conducted to characterize crystal structures, phase, and orientations of SnOx films, using the PANalytical X'Pert PRO diffractometer and the out-of-plane 2θ-scan method. Morphologies of films were also characterized by atomic force microscopy microscopy (AFM, NT-MDT, NTEGRA). X-ray photoelectron spectroscopy (XPS) analyses were used to characterize the chemical compositions and oxidation states of SnOx films. XPS was conducted on a Thermo Scientific Theta Probe system with the monochromatic Al Kα X-ray source ($h\nu$ = 1486.6 eV). The van der Pauw and Hall-effect measurements were used to characterize electrical properties of SnOx films, such as resistivity, carrier type, carrier mobility, and carrier concentration. They were conducted on a Nanometrics HL5500 system with a high-impedance buffer amplifier/current source. Optical properties of films (transmission/reflection/absorption spectra etc.) were characterized with a UV−visible spectrometer (Hitachi, U-4100).

The schematic device structure of bottom-gate p-type SnO TFTs studied in this work is shown in Figure 1. The heavily doped n-type Si wafer served both as the substrate and as the bottom gate. The gate insulator used was a 200 nm-thick thermally grown SiO_2 layer on the Si substrate. Patterned SnO films (30 nm thick) were deposited and patterned through shadow masks. Metal source/drain (S/D) electrodes were subsequently deposited and patterned by e-beam evaporation through shadow masks. Pure Mo was adopted in this study as S/D electrodes, which had been demonstrated to have good contact characteristics with p-type SnO thin films in a previous study.[16] The width of the SnO islands defined the channel width (W = 500 μm), while the spacing between S/D electrodes defined the channel length (L = 200 μm) for TFTs in this work. Finally, the completed TFTs were subjected to a postannealing at 200−300 °C in vacuum in a RTA system for 1 h. Device characteristics were then measured using an Agilent 4155B Semiconductor Parameter Analyzer.

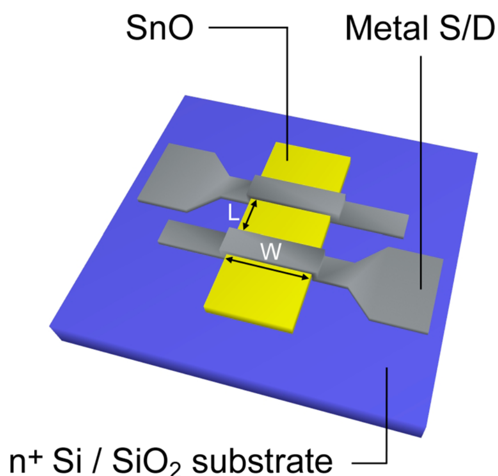

Figure 1. Schematic device structure of the p-type SnO TFT.

3. RESULTS AND DISCUSSIONS

Figure 2 shows XRD patterns of 100 nm-thick SnO_X films sputtered from the SnO_2 target with varied H_2 gas ratios of 0−50% in the mixed Ar/H_2 atmosphere (with a RF power of 200 W, a working pressure of 5 mTorr) and being subjected to postannealing at 300 °C in vacuum for 1 h. By sputtering with pure Ar or low H_2 ratios (i.e., 0−25%), XRD patterns of films remained broad and featureless even after 300 °C postannealing, indicating the films still be of amorphous nature and reveal no evident sign of any SnOx phase yet. Yet, further increasing the H_2 gas ratio to 33.3% in sputtering, clear XRD peaks were observed. These XRD peaks can be unambiguously assigned to those of the α-SnO crystal structure, which has a tetragonal unit cell with a PbO litharge structure (space group: $P4/nmm$) and is featured by a $Sn_{1/2}$−O−$Sn_{1/2}$ layer sequence and a van der Waals gap between two adjacent Sn planes along the [001] crystallographic direction.[18] The hardly visible signals from either the β-Sn or the SnO_2 phase (in XRD patterns of the 33.3% sample) indicates the combination of the SnO_2 target and the Ar/H_2 mixed gas be effective for sputtering deposition of rather SnO-dominant films/phase. Increasing the H_2 gas ratio further to 40% and 50%, along with the α-SnO signals, XRD peaks associated with the β-Sn phase emerged and became visible.[14] XRD results suggest that an appropriate/sufficient amount of H_2 in the sputtering gas can indeed successfully reduce SnO_2 into SnO, whereas excess H_2 would result in over reduction of SnO_2 into metallic Sn.

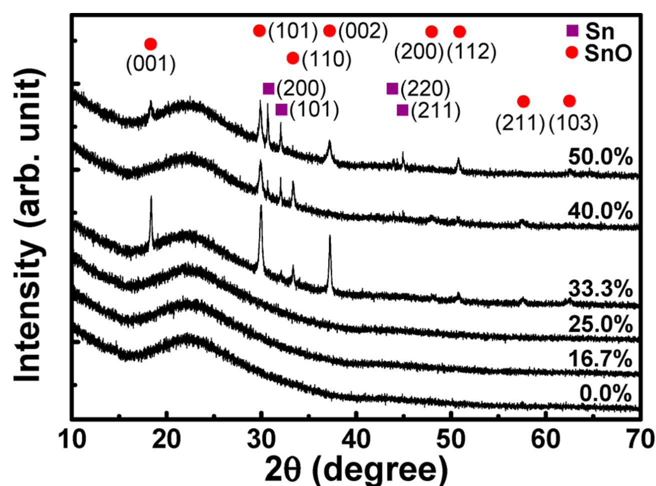

Figure 2. XRD patterns of SnOx films deposited with different H_2 gas ratios (and subjected to annealing at 300 °C).

Morphologies of films were further characterized by AFM. Figure 3a shows the topographical AFM images of SnO_X films deposited with varied H_2 gas ratios after postannealing at 300 °C. The evolution of morphologies observed in AFM appears consistent with that observed in XRD. Surfaces of SnOx films deposited with 0−25% H_2 ratios (that showed no XRD

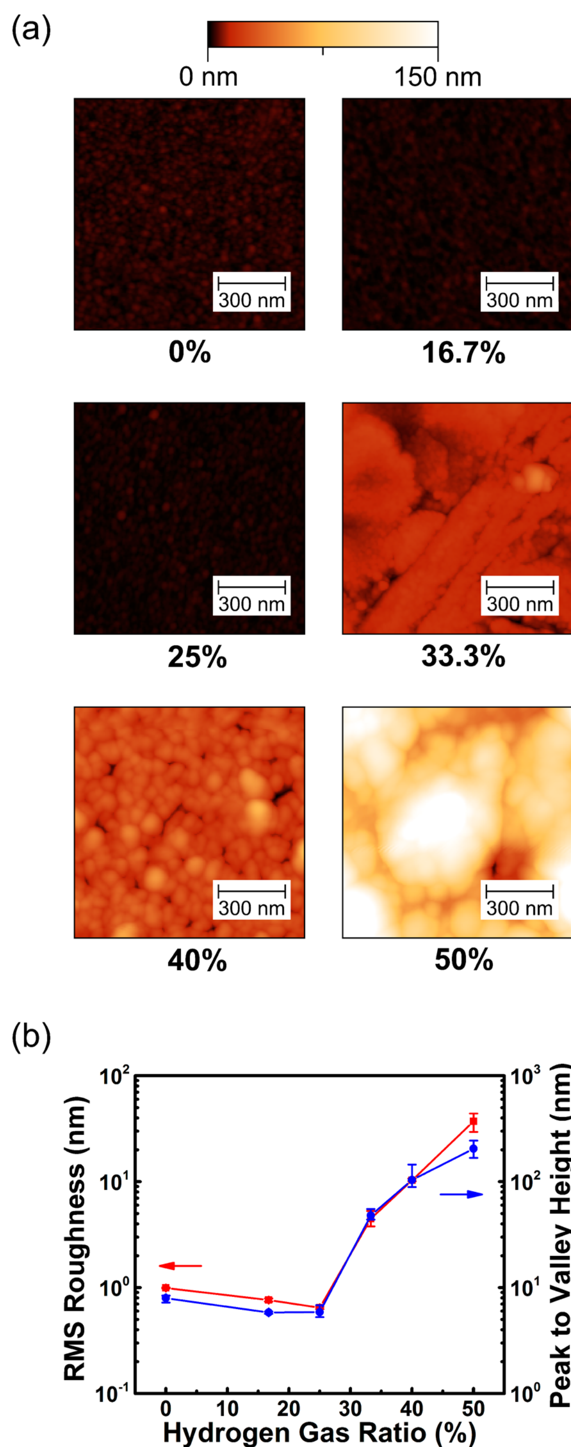

Figure 3. (a) AFM images of 300 °C-annealed SnO_X films deposited with different H_2 gas ratios. (b) RMS surface roughness and peak-to-valley height of SnO_X films deposited with different H_2 gas ratios.

patterns) are featureless, smooth, and of amorphous nature. Meanwhile surface textures/grains presumably associated with crystallization are visible in samples deposited with H_2 gas ratios of 33.3−50% (that showed strong XRD patterns). Figure 3b shows the root-mean-square (RMS) surface roughness and the peak-to-valley height of SnOx films as a function of the H_2 gas ratio. It clearly reveals a takeoff of the more dramatic morphological change at the H_2 gas ratio around 33.3%. At the highest H_2 gas ratios investigated (50%), the surfaces were very rough and the peak-to-valley height could be as high as ∼200 nm

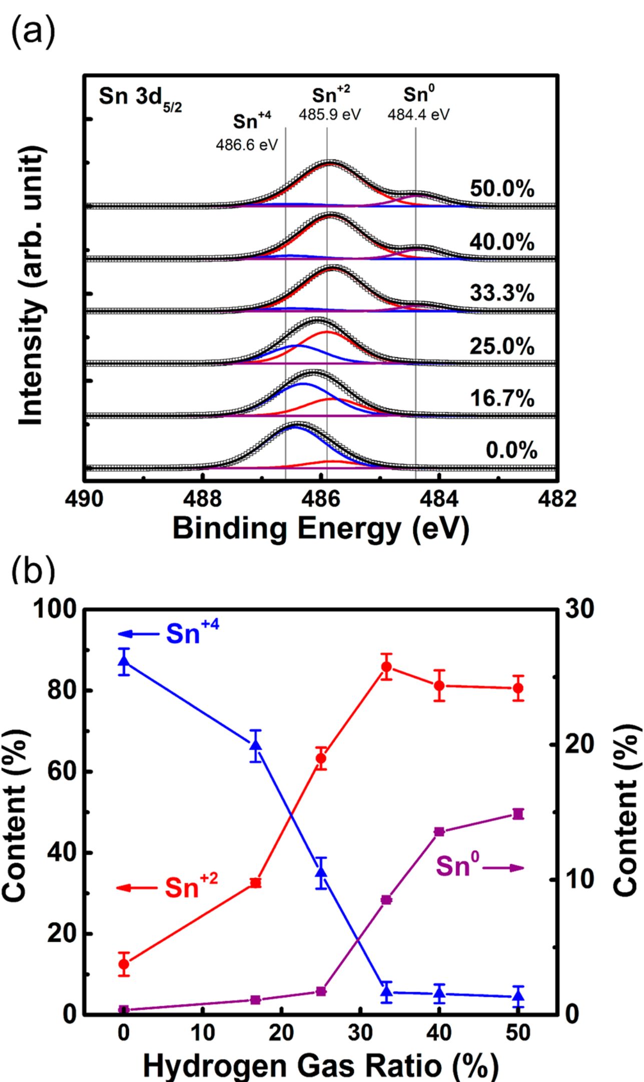

Figure 4. (a) XPS spectra in the Sn $3d_{5/2}$ core-level region for SnO_X films deposited with varied H_2 gas ratios. Deconvoluted Sn^0, Sn^{2+}, and Sn^{4+} components (purple, red, and blue lines, respectively) to fit measured Sn $3d_{5/2}$ core-level spectra are also shown. (b) The contents of Sn^0 (purple), Sn^{2+} (red), and Sn^{4+} (blue) components in SnO_X films (derived from Sn $3d_{5/2}$ core-level spectra) as a function of the H_2 gas ratio.

SnO_X films deposited with varied H_2 gas ratios were further investigated by XPS to characterize their chemical compositions and oxidation states. Figure 4a shows the XPS spectra in the Sn $3d_{5/2}$ core-level region for the 300 °C-annealed SnO_X films sputtered with varied H_2 gas ratios. The chemical compositions and the oxidation states of Sn (i.e., Sn^0, Sn^{2+} or Sn^{4+}) in these films can be quantitatively examined by deconvoluting the observed Sn $3d_{5/2}$ core-level spectra with Sn^0, Sn^{2+}, and Sn^{4+} components. The best-fit curves for different H_2 gas ratios are also illustrated in Figure 4a. The best fitting achieved suggests the Sn^0, Sn^{2+} and Sn^{4+} components are located around 484.4, 485.9, and 486.6 eV, respectively. The chemical shifts toward higher binding energy are about 2.2 eV from Sn^0 to Sn^{4+} and 0.7 eV from Sn^{2+} to Sn^{4+}. These binding energies and chemical shifts well agree with the results previously reported.[19,20] In increasing the H_2 gas ratio from 0% to 25%, peaks of the Sn

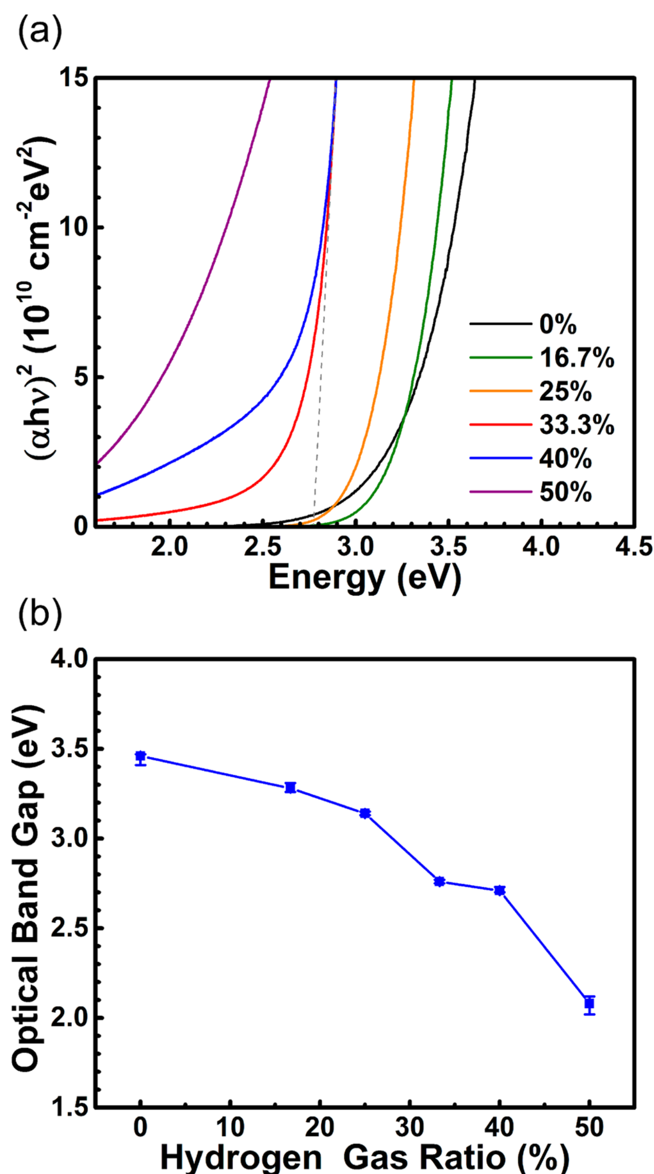

Figure 5. (a) $(\alpha h\nu)^2$ vs $h\nu$ plots of SnOx films sputtered with varied H_2 gas ratios. (b) Optical bandgaps of SnOx films as a function of the H_2 gas ratio.

Table 1. Electrical Properties of SnOx Films Deposited with Different H_2 Gas Ratios

hydrogen gas ratio (%)	Hall mobility (cm^2 V^{-1} s^{-1})	hole concentration (cm^{-3})	resistivity (Ω cm)
0	N/A	N/A	1×10^5 to 1×10^6
16.7	N/A	N/A	1×10^7 to 1×10^8
25	N/A	N/A	1×10^7 to 1×10^8
33.3	1.02	5.86×10^{18}	1.05
40	3.00	7.22×10^{16}	31.54
50	N/A	N/A	1×10^7 to 1×10^8

$3d_{5/2}$ spectra evolve from being closer to 486.6 eV to being closer to 485.9 eV, indicating an evolution from the dominance of the Sn^{4+}/SnO_2 oxidation/valency state to the coexistence of Sn^{2+}/SnO and Sn^{4+}/SnO2 oxidation/valency states in SnO_X

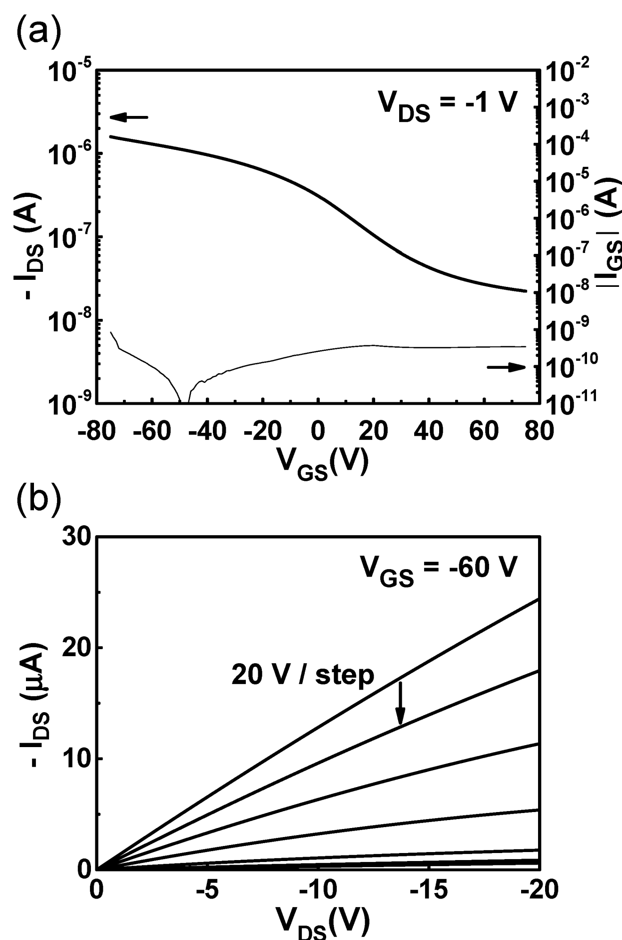

Figure 6. (a) Transfer and (b) output characteristics of the p-type SnO TFT (W/L = 500/200 μm) using the SnO-dominant film deposited with the 33.3% H_2 gas ratio.

films. Further increasing the H_2 gas ratio to 33.3% and beyond, the spectra become mainly composed of a dominant Sn^{2+} component and an increasing Sn^0 component. From fitting results of Figure 4a, the contents of Sn^0, Sn^{2+} and Sn^{4+} components as a function of the H_2 gas ratio in sputtering are derived and are plotted in Figure 4b. The content of Sn^{4+}/SnO_2 initially dominates with sputtering in pure Ar. With the increase of the H_2 ratio, the content of Sn^{4+}/SnO_2 continuously drops and becomes negligible (<6%) at the H_2 ratio of ≥33.3%. The content of Sn^{2+}/SnO first rises with the H_2 gas ratio and reaches the maximum (~86%) and becomes dominant at the H_2 ratio of 33.3%. The content of Sn^{2+}/SnO gradually decreases at even higher H_2 ratios. This is mainly associated with the apparent increase of the Sn^0 content at such higher H_2 ratios, mostly because of increasingly stronger reduction capability of the sputtering gas.

Overall, the introduction of an appropriate amount of hydrogen into the sputtering gas is effective to control valency/oxidation states of Sn in SnO_X films sputtered from the SnO_2 target. The Sn^{4+}/SnO_2 phase is effectively suppressed with an appropriate ratio of H_2 in Ar (e.g., 33.3%) and a Sn^{2+}/SnO-dominant film could be obtained. This is presumably associated with the strong chemical reducing capability of the hydrogen plasma during sputtering.[21,22] Too much hydrogen in the sputtering gas, however, may make the reducing capability too strong so that SnOx is over reduced to yield neutral Sn, as already signaled by the increased Sn content at the highest H_2

dx.doi.org/10.1021/am5031787 | ACS Appl. Mater. Interfaces 2014, 6, 13724−13729

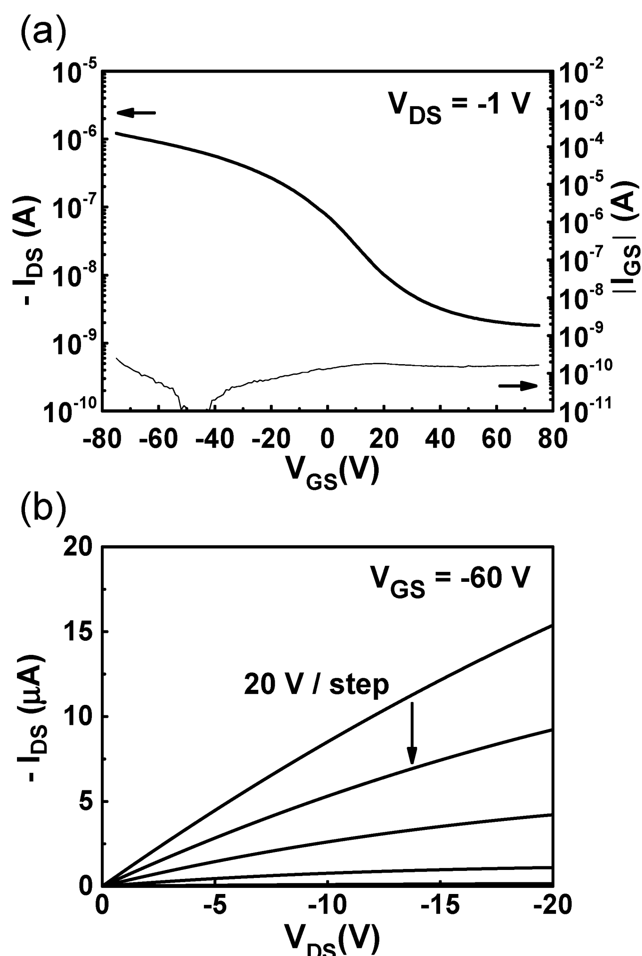

Figure 7. (a) Transfer and (b) output characteristics of the p-type SnO TFTs (W/L = 500/200 μm) using the SnO-dominant film deposited with the 40% H_2 gas ratio.

ratios (i.e., 40%, 50%) investigated. While SnOx films containing mixture of SnO_2 and SnO tend to remain amorphous (or at least no XRD-detectable crystallinity) even with annealing at 300 °C, SnO-dominant films in general show clear XRD patterns and crystallinity of the tetragonal α-SnO crystal structure with annealing at 300 °C.

The direct optical bandgaps of SnOx films deposited with varied H_2 gas ratios were evaluated from their $(\alpha h\nu)^2$ vs $h\nu$ plots as shown in Figure 5a,[12] where α and $h\nu$ are the absorption coefficient and the photon energy, respectively. The absorption coefficient α was extracted from measured reflectance (R) and transmittance (T) via the relationship: $T/(1 - R) = e^{-\alpha l}$,[23] where l is the thickness of the film. By linearly extrapolating the $(\alpha h\nu)^2$ curve to the horizontal axis, the apparent direct optical bandgaps of SnOx films are derived and are shown in Figure 5b. As the H_2 gas ratio increases, the optical bandgap decreases continuously from ~3.16−3.46 eV (for pure Ar or low H_2 gas ratio) to 2.71−2.76 eV (for H_2 gas ratios of 33.3% or 40%) and then to 2.08 eV (for H_2 gas ratio of 50%). Upon considering the very different optical properties of SnO_2, SnO, and metallic Sn, such a trend is indeed consistent with the compositional transition in SnOx films (as manifested in Figure 4). SnO_2 in general has a larger optical bandgap of ~3.6 eV,[24] SnO has been reported to have a direct optical bandgap of ~2.7 eV,[12] and metallic Sn clusters in films would induce strong absorption over a wide wavelength range.[19] As such, with evolution from SnO_2-dominant, SnO_2/SnO mixture, SnO-dominant, to SnO/Sn mixture compositions, one observes an apparent decrease of the optical bandgap with the H_2 gas ratio.

Electrical properties (e.g., resistivity, carrier type, carrier mobility, carrier concentration) of 300 °C-annealed SnOx films deposited with varied H_2 gas ratios were characterized by van der Pauw and Hall-effect measurements and are summarized in Table 1. The 0, 16.7, and 25% samples (having SnO_2/SnO mixed phase and appearing amorphous) showed rather high resistivity of ~1×10^5 to 1×10^8 Ω cm, making it not possible to determine the carrier mobility and concentration. 33.3% and 40% samples unambiguously showed p-type conductivity, coincident with the detected poly crystalline SnO phase in XRD (Figure 2). P-type Hall mobilities and carrier concentrations of 33.3% and 40% samples were (1.02 $cm^2\ V^{-1}\ s^{-1}$, 5.86×10^{18} cm^{-3}) and (3 $cm^2\ V^{-1}\ s^{-1}$, 7.22×10^{16} cm^{-3}), respectively. The traceable Sn^0 component (as revealed in Figure 4) and the β-Sn phase (as revealed in Figure 2) in these films do not seem to hinder the observation of p-type conductivity. Indeed the 40% sample having more Sn^0/β-Sn embedded in the SnO matrix shows higher mobility than the more SnO-dominant 33.3% sample. Similar observations have been previously reported in p-type SnO grown by other techniques (e.g., SnO grown by sputtering with the Sn target in an oxygen-containing/oxidizing atmosphere).[14] Previous theoretical studies had indicated that native defeats like Sn interstitials and O vacancies in the Sn-rich environment could modify the valence band, inducing higher contributions of delocalized Sn 5p orbitals as compared to localized O 2p orbitals and thus increasing hole mobility.[25] The p-type carrier mobility obtained here is roughly comparable with those obtained with reactive sputtering from the Sn target,[14,19] but the SnO_2 target used here may be more robust than the Sn target for heavy-loading depositions. For the SnOx film deposited with the highest H_2 gas ratio of 50%, again the resistivity was too high for determination of carrier mobility and concentration. Its high resistivity may be associated with the huge roughness and thus poorer quality of the film.

Finally, bottom-gate p-type SnO TFTs were fabricated using 30 nm-thick SnO-dominant films deposited with the SnO_2 target at 33.3% and 40% H_2 gas ratios and postannealed at 200−300 °C for 1 h. In this annealing temperature range, it was generally observed that the TFT field-effect mobilities (μ_{FE}) decreased and the on/off ratios increased with the annealing temperature. Compromise of these two TFT characteristics was obtained around the annealing temperature of 260 °C, and representative TFT characteristics with this annealing temperature are presented below (Figures 6 and 7). With annealing at 260 °C, the 30 nm films deposited with 33.3% and 40% H_2 gas ratios exhibited a RMS surface roughness of 0.8−1.2 nm and a peak-to-valley height of 6.5−9 nm. The lower annealing temperature needed for TFTs than for films may be associated with the smaller film thickness in TFTs, the off current requirement, and difference in carrier transport mechanisms (i.e., carrier transport near the dielectric interface vs bulk film transport etc.). Figure 6 shows the transfer and output characteristics of the p-type SnO TFTs using the SnO-dominant film deposited with the 33.3% H_2 gas ratio and postannealed at 260 °C. The TFT showed clear gate-modulated drain current (I_{DS}) characteristics of a p-channel TFT. From I−V characteristics shown in Figure 6, one extracts an on/off ratio of 7.11×10^1 and a linear μ_{FE} of 0.42 $cm^2\ V^{-1}$

s^{-1}. Figure 7 shows the transfer and output characteristics of the p-type SnO TFTs using the SnO-dominant film deposited with the 40% H_2 gas ratio and postannealed at 260 °C. It gives a μ_{FE} of 0.43 $cm^2\ V^{-1}\ s^{-1}$ and an on/off ratio of 6.70×10^2. Both p-channel TFTs show similar field-effect mobilities, but the TFT using the film deposited with the 40% H_2 ratio gives a higher on/off ratio, presumably due to the lower carrier concentration in the 40% film (as revealed by the Hall-effect measurement). The slightly larger gate-leakage currents (i.e., 1×10^{-9} to 1×10^{-11} A) in these devices were due to the relatively large dimensions of the devices and overlaps between gates and S/D electrodes. Nevertheless, they were still much smaller than the drain current and did not disturb observation of transistor characteristics.

4. CONCLUSIONS

In conclusion, we had investigated sputtering deposition of p-type SnO using the widely used and robust SnO_2 target in a hydrogen-containing reducing atmosphere. The effects of the hydrogen-containing sputtering gas on structures, compositions, optical, and electrical properties of deposited SnOx films were studied. Results show that polycrystalline and p-type SnO-dominant films could be readily obtained by carefully controlling the hydrogen gas ratio in the sputtering gas and the extent of reduction reaction. The SnO-dominant films thus obtained exhibited a p-type Hall mobility of up to ~3 $cm^2\ V^{-1}\ s^{-1}$. P-type SnO TFTs using such SnO-dominant films were also demonstrated, showing a field-effect mobility of 0.43 $cm^2\ V^{-1}\ s^{-1}$.

■ AUTHOR INFORMATION

Corresponding Author

*E-mail: wucc@ntu.edu.tw.

Present Address

§H.-H.H. is currently at Polyera Taiwan Corp., Hsinchu 302, Taiwan

Notes

The authors declare no competing financial interest.

■ ACKNOWLEDGMENTS

The authors gratefully acknowledge the financial support from Ministry of Science and Technology (Grant 100-2622-E-002-004-CC2 and 101-2221-E-002-158-MY3) and Ministry of Education of Taiwan (Grant 103R7607-2).

■ REFERENCES

(1) Nomura, K.; Ohta, H.; Takagi, A.; Kamiya, T.; Hirano, M.; Hosono, H. Room-temperature fabrication of transparent flexible thin-film transistors using amorphous oxide semiconductors. *Nature* **2004**, *432*, 488−492.

(2) Yabuta, H.; Sano, M.; Abe, K.; Aiba, T.; Den, T.; Kumomi, H.; Nomura, K.; Kamiya, T.; Hosono, H. High-mobility thin-film transistor with amorphous InGaZnO4 channel fabricated by room temperature rf-magnetron sputtering. *Appl. Phys. Lett.* **2006**, *89* (112123), 1−3.

(3) Fortunato, E.; Barquinha, P.; Martins, R. Oxide Semiconductor Thin-Film Transistors: A Review of Recent Advances. *Adv. Mater.* **2012**, *24*, 2945−2986.

(4) Kawazoe, H.; Yasukawa, M.; Hyodo, H.; Kurita, M.; Yanagi, H.; Hosono, H. P-type electrical conduction in transparent thin films of CuAlO2. *Nature* **1997**, *389*, 939−942.

(5) Kudo, A.; Yanagi, H.; Hosono, H.; Kawazoe, H. SrCu2O2: A p-type conductive oxide with wide band gap. *Appl. Phys. Lett.* **1998**, *73*, 220−222.

(6) Sato, H.; Minami, T.; Takata, S.; Yamada, T. Transparent conducting p-type Nio thin-films prepared by magnetron sputtering. *Thin Solid Films* **1993**, *236*, 27−31.

(7) Musa, A. O.; Akomolafe, T.; Carter, M. J. Production of cuprous oxide, a solar cell material, by thermal oxidation and a study of its physical and electrical properties. *Sol. Energy Mater. Sol. Cells* **1998**, *51*, 305−316.

(8) Pan, X. Q.; Fu, L. Tin Oxide Thin Films Grown on the (¯1012) Sapphire Substrate. *J. Electroceram.* **2001**, *7*, 35−46.

(9) Chang, P. C.; Fan, Z. Y.; Tseng, W. Y.; Rajagopal, A.; Lu, J. G. β-Ga2O3 nanowires: Synthesis, characterization, and p-channel field-effect transistor. *Appl. Phys. Lett.* **2005**, *87* (222102), 1−3.

(10) Shimotani, H.; Suzuki, H.; Ueno, K.; Kawasaki, M.; Iwasa, Y. p-type field-effect transistor of NiO with electric double-layer gating. *Appl. Phys. Lett.* **2008**, *92* (242107), 1−3.

(11) Matsuzaki, K.; Nomura, K.; Yanagi, H.; Kamiya, T.; Hirano, M.; Hosono, H. Epitaxial growth of high mobility Cu2O thin films and application to *p*-channel thin film transistor. *Appl. Phys. Lett.* **2008**, *93* (202107), 1−3.

(12) Ogo, Y.; Hiramatsu, H.; Nomura, K.; Yanagi, H.; Kamiya, T.; Hirano, M.; Hosono, H. *p*-channel thin-film transistor using p-type oxide semiconductor, SnO. *Appl. Phys. Lett.* **2008**, *93* (032113), 1−3.

(13) Ogo, Y.; Hiramatsu, H.; Nomura, K.; Yanagi, H.; Kamiya, T.; Kimura, M.; Hirano, M.; Hosono, H. Tin monoxide as an s-orbital-based p-type oxide semiconductor: Electronic structures and TFT application. *Phys. Status Solidi A* **2009**, *206*, 2187−2191.

(14) Fortunato, E.; Barros, R.; Barquinha, P.; Figueiredo, V.; Park, S. H. K.; Hwang, C. S.; Martins, R. Transparent p-type SnOx thin film transistors produced by reactive rf magnetron sputtering followed by low temperature annealing. *Appl. Phys. Lett.* **2010**, *97* (052105), 1−3.

(15) Yabuta, H.; Kaji, N.; Hayashi, R.; Kumomi, H.; Nomura, K.; Kamiya, T.; Hirano, M.; Hosono, H. Sputtering formation of *p*-type SnO thin-film transistors on glass toward oxide complimentary circuits. *Appl. Phys. Lett.* **2010**, *97* (072111), 1−3.

(16) Hsu, P. C.; Chen, W. C.; Tsai, Y. T.; Kung, Y. C.; Chang, C. H.; Hsu, C. J.; Wu, C. C.; Hsieh, H. H. Fabrication of p-Type SnO Thin-Film Transistors by Sputtering with Practical Metal Electrodes. *Jpn. J. Appl. Phys.* **2013**, *52* (05DC07), 1−6.

(17) Hosono, H.; Ogo, Y.; Yanagi, H.; Kamiya, T. Bipolar Conduction in SnO Thin Films. *Electrochem. Solid-State Lett.* **2011**, *14*, H13−H16.

(18) Batzill, M.; Diebold, U. The surface and materials science of tin oxide. *Prog. Surf. Sci.* **2005**, *79*, 47−154.

(19) Luo, H.; Liang, L. Y.; Cao, H. T.; Liu, Z. M.; Zhuge, F. Structural, Chemical, Optical, and Electrical Evolution of SnOx Films Deposited by Reactive rf Magnetron Sputtering. *ACS Appl. Mater. Interfaces* **2012**, *4*, 5673−5677.

(20) Kover, L.; Kovacs, Z.; Sanjines, R.; Moretti, G.; Cserny, I.; Margaritondo, G.; Palinkas, J.; Adachi, H. Electronic-Structure of Tin Oxides: High-Resolution Study of Xps and Auger-Spectra. *Surf. Interface Anal.* **1995**, *23*, 461−466.

(21) Zhang, K. R.; Zhu, F. R.; Huan, C. H. A.; Wee, A. T. S. Effect of hydrogen partial pressure on optoelectronic properties of indium tin oxide thin films deposited by radio frequency magnetron sputtering method. *J. Appl. Phys.* **1999**, *86*, 974−980.

(22) Zhang, K.; Zhu, F. R.; Huan, C. H. A.; Wee, A. T. S. Indium tin oxide films prepared by radio frequency magnetron sputtering method at a low processing temperature. *Thin Solid Films* **2000**, *376*, 255−263.

(23) Hishikawa, Y.; Nakamura, N.; Tsuda, S.; Nakano, S.; Kishi, Y.; Kuwano, Y. Interference-Free Determination of the Optical-Absorption Coefficient and the Optical Gap of Amorphous-Silicon Thin-Films. *Jpn. J. Appl. Phys.* **1991**, *30*, 1008−1014.

(24) Melsheimer, J.; Ziegler, D. Band-Gap Energy and Urbach Tail Studies of Amorphous, Partially Crystalline and Polycrystalline Tin Dioxide. *Thin Solid Films* **1985**, *129*, 35−47.

(25) Granato, D. B.; Caraveo-Frescas, J. A.; Alshareef, H. N.; Schwingenschlogl, U. Enhancement of p-type mobility in tin monoxide by native defects. *Appl. Phys. Lett.* **2013**, *102* (212105), 1−4.